doi:10.1016/j.jmb.2009.06.063 J. Mol. Biol. (2009) 391, 784–796

JMB

Available online at www.sciencedirect.com

ScienceDirect

ELSEVIER

Structural Reorganization of α-Synuclein at Low pH Observed by NMR and REMD Simulations

Kuen-Phon Wu[1], Daniel S. Weinstock[2], Chitra Narayanan[3], Ronald M. Levy[1,2*] and Jean Baum[1,2*]

[1]*Department of Chemistry and Chemical Biology, Rutgers University, 610 Taylor Road, Piscataway, NJ 08854, USA*

[2]*BioMaPS Institute for Quantitative Biology, Rutgers University, Piscataway, NJ 08854, USA*

[3]*Graduate Program in Biochemistry, Rutgers University, Piscataway, NJ 08854, USA*

Received 3 March 2009; received in revised form 4 June 2009; accepted 25 June 2009
Available online 1 July 2009

α-Synuclein is an intrinsically disordered protein that appears in aggregated forms in the brains of patients with Parkinson's disease. The conversion from monomer to aggregate is complex, and aggregation rates are sensitive to changes in amino acid sequence and environmental conditions. It has previously been observed that α-synuclein aggregates faster at low pH than at neutral pH. Here, we combine NMR spectroscopy and molecular simulations to characterize α-synuclein conformational ensembles at both neutral and low pH in order to understand how the altered charge distribution at low pH changes the structural properties of these ensembles and leads to an increase in aggregation rate. The N-terminus, which has a small positive charge at neutral pH due to a balance of positively and negatively charged amino acid residues, is very positively charged at low pH. Conversely, the acidic C-terminus is highly negatively charged at neutral pH and becomes essentially neutral and hydrophobic at low pH. Our NMR experiments and replica exchange molecular dynamics simulations indicate that there is a significant structural reorganization within the low-pH ensemble relative to that at neutral pH in terms of long-range contacts, hydrodynamic radius, and the amount of heterogeneity within the conformational ensembles. At neutral pH, there is a very heterogeneous ensemble with transient contacts between the N-terminus and the non-amyloid β component (NAC); however, at low pH, there is a more homogeneous ensemble that exhibits strong contacts between the NAC and the C-terminus. At both pH values, transient contacts between the N- and C-termini are observed, the NAC region shows similar exposure to solvent, and the entire protein shows similar propensities to secondary structure. Based on the comparison of the neutral- and low-pH conformational ensembles, we propose that exposure of the NAC region to solvent and the secondary-structure propensity are not factors that account for differences in propensity to aggregate in this context. Instead, the comparison of the neutral- and low-pH ensembles suggests that the change in long-range interactions between the low- and neutral-pH ensembles, the compaction of the C-terminal region at low pH, and the uneven distribution of charges across the sequence are key to faster aggregation.

Keywords: Parkinson's disease; α-synuclein; NMR; replica exchange molecular dynamics

Edited by P. Wright

*Corresponding authors. E-mail addresses: ronlevy@lutece.rutgers.edu; jean.baum@rutgers.edu.

Abbreviations used: PD, Parkinson's disease; NAC, non-amyloid β component; IDP, intrinsically disordered protein; R_2^{CPMG}, CPMG-type transverse relaxation; RDC, residual dipolar coupling; PRE, paramagnetic relaxation enhancement; MTSL, (1-oxy-2,2,5,5-tetra-methyl-3-pyrroline-3-methyl)-methanesulfonate; REMD, replica exchange molecular dynamics; SASA, solvent-accessible surface areas; C8E5, pentaethylene glycol monooctyl ether; HSQC, heteronuclear single quantum coherence; PFG, pulsed-field gradient; PBS, phosphate-buffered saline; PFG-NMR, pulsed-field gradient NMR.

0022-2836/$ - see front matter. Published by Elsevier Ltd.

Introduction

Many human diseases are associated with proteins that convert from their normally soluble form to aggregates that accumulate in the affected organs. The final forms of the aggregates include fibrillar plaques known as amyloid. This disease class includes Alzheimer's disease, Parkinson's disease (PD), Huntington's disease, prion disease, and type II diabetes.[1–4] PD is the second most prevalent of the late-onset neurodegenerative diseases.[5] α-Synuclein is the primary protein component of the Lewy body deposits that are the diagnostic hallmark of PD and is expressed in high levels in the brain.[6] α-Synuclein can adopt two forms, the free form found in the cytoplasm and a highly helical membrane-bound form.[7,8] The membrane-bound α-synuclein may be crucial for physiological functions[9–12] and has been shown to be associated with the recruitment of dopamine in the presynapse and with the synaptic signal transmission.[13] The aggregation of α-synuclein has been shown to occur via a nucleation-dependent mechanism during which there is an initial lag phase followed by a growth phase.[14] The rate of fibrillization is highly dependent on the sequence identity of the protein as well as the solution conditions, and the details of the mechanism remain unclear.

One approach to understanding the progression of fibril formation is to study human α-synuclein and variants under different conditions in order to define the distribution of conformational states in the monomeric ensemble and how these may be related to the aggregation propensities. Human α-synuclein in the free form has been shown to be an intrinsically disordered protein (IDP)[15,16] and, similar to other IDPs, is characterized by a low sequence complexity, low overall hydrophobicity, and high net charge.[17] It consists of three regions: an N-terminal region (residues 1–60) with a highly conserved hexamer motif KTKEGV forms α-helices in association with membranes.[8,18,19] A central hydrophobic region, known as the "non-amyloid β component" (NAC) (residues 61–95), is proposed to be primarily responsible for aggregation.[20] The C-terminal region (residues 96–140) is acidic, proline-rich,[21] and also contains three highly conserved tyrosine residues. The charged residues are unevenly distributed within the sequence (Fig. 1) and result in a net charge of −9 at neutral pH (Table 1). The N-terminus has a high charge density at neutral pH (18 charged residues out of 60), but the balance between positive and negative charges leads to a net charge of +4, while the NAC, with a net charge of −1, only has three charged residues. The C-terminus at neutral pH has an even higher percentage of charged residues than the N-terminus (18 out of 45 residues), and a preponderance of negatively charged Asp and Glu residues results in a net charge of −12. The uneven distribution of charges within the three regions implies that the charge profile of α-synuclein is strongly dependent on pH.

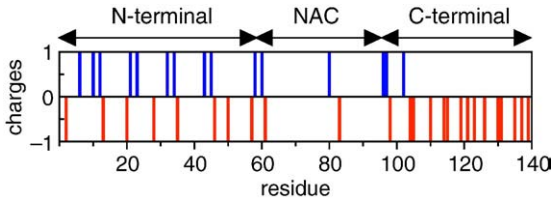

Fig. 1. Distribution of charged residues of α-synuclein. The distribution of positive (blue) and negative (red) charged residues of α-synuclein at pH 7.4 is shown.

The charge distribution of the NAC, which has very few charged residues, is not greatly affected by the change in pH. However, the N-terminus region that contains the highest fraction of positively charged residues becomes the region with the highest charge density at low pH, while the C-terminus, at low pH, becomes more like the NAC, with both a low charge density and a low net charge.

Developing a better understanding of how sequence-dependent effects alter the conformational propensities of monomeric α-synuclein, and correlating these effects with changes in aggregation rates, can provide insights into the mechanistic basis for abnormal folding and human disease. The conformational states of the synuclein family, consisting of human α-synuclein,[15] β-synuclein,[22,23] and γ-synuclein,[24] as well as the familial mutations of synuclein A53T,[25,26] A30P,[25,26] and E46K[27,28] and mouse α-synuclein,[29] which contains seven mutations relative to human α-synuclein, have been studied extensively using NMR and other spectroscopic approaches. Human α-synuclein at neutral pH has a relatively more compact conformation than is expected for a random-coil conformation, and transient α-helical structure has been detected in the N-terminal region of the protein.[22,23,29–31] Transient long-range interactions between the C- and N-terminal regions and also between the C-terminal and NAC regions have been proposed based on paramagnetic relaxation enhancement (PRE) measurements.[23,29,30,32,33] Observation of these long-range interactions has led to the proposal that the contacts between the NAC and the C-terminal regions shield the hydrophobic NAC region and therefore delay the aggregation of α-synuclein under these conditions.[23,30,32] Destabilization of these long-range contacts in mouse α-synuclein[29] and in A53T and A30P mutations[25] involved in early-onset disease has been correlated with faster aggregation, supporting the notion that protection of the NAC region may be important for delaying aggregation.[25] An alternative view is that there is little difference in long-range contacts between the wild type and mutant forms of α-synuclein and that changes in aggregation rate can be attributed to local changes in the physicochemical properties of individual residues.[28]

At low pH, α-synuclein has been shown to aggregate faster than at neutral pH, with fibrils taking days to form rather than several weeks.[31] Uversky

Table 1. Distribution of charges in the sequence of α-synuclein

	N			NAC			C			α-Synuclein		
pH	Net	Total	%	Net	Total	%	Net	Total	%	Net	Total	%
Neutral	+4	18	30.0	−1	3	8.6	−12	18	40.0	−9	39	27.8
Low	+11	11	18.3	+1	1	2.9	+3	3	6.7	+15	15	10.7

The table shows the net charge, total charge (total number of charged residues), and percentage of charged residues in the N, NAC, and C regions and the full α-synuclein sequence at neutral pH and low pH.

et al. have observed, via CD, Fourier transform infrared spectroscopy, and small-angle X-ray scattering measurements, a 1.3-fold compaction in the radius of gyration of α-synuclein at low pH as well as an increase in β structure.[31] They have suggested that the compaction of the protein into a partially folded conformation is responsible for the increased rate of aggregation at low pH.

NMR spectroscopy[34–37] and computer simulations[38–40] have been developed in recent years to characterize conformational ensembles of IDPs. Here, we use NMR and computational approaches to compare the conformational ensembles of α-synuclein at neutral and low pH. These studies help identify the role of electrostatic interactions in the pH-dependent structural changes of α-synuclein and relate these to the different aggregation propensities as a function of pH. The NMR measurements, when combined with structures generated by computer simulations, provide the first visualization of the conformational ensemble of α-synuclein at low pH. The results suggest that there is a significant structural reorganization relative to the neutral-pH ensemble in terms of long-range intra-chain contacts and hydrodynamic radius. At neutral pH, the highly charged C-terminal tail makes contact with the other regions of the protein in only a small population of structures. In contrast, at low pH, the C-terminus is locally collapsed. The secondary-structure propensity and exposure of the NAC region to solvent are not affected by the pH change. The structural changes observed at low pH highlight the effects that the very different charge characteristics in the N-terminal, NAC, and C-terminal chain segments have on the pH-dependent structural reorganization of α-synuclein.

Results

Acid-induced changes in structure and dynamics probed by NMR

The ^{1}H–^{15}N heteronuclear single quantum coherence (HSQC) spectrum at pH 2.5 and 15 °C exhibits similar spectral features to the HSQC spectrum at pH 7.4;[15] the narrow $^{1}H^{N}$ chemical shift range and poor dispersion suggest that α-synuclein is intrinsi-

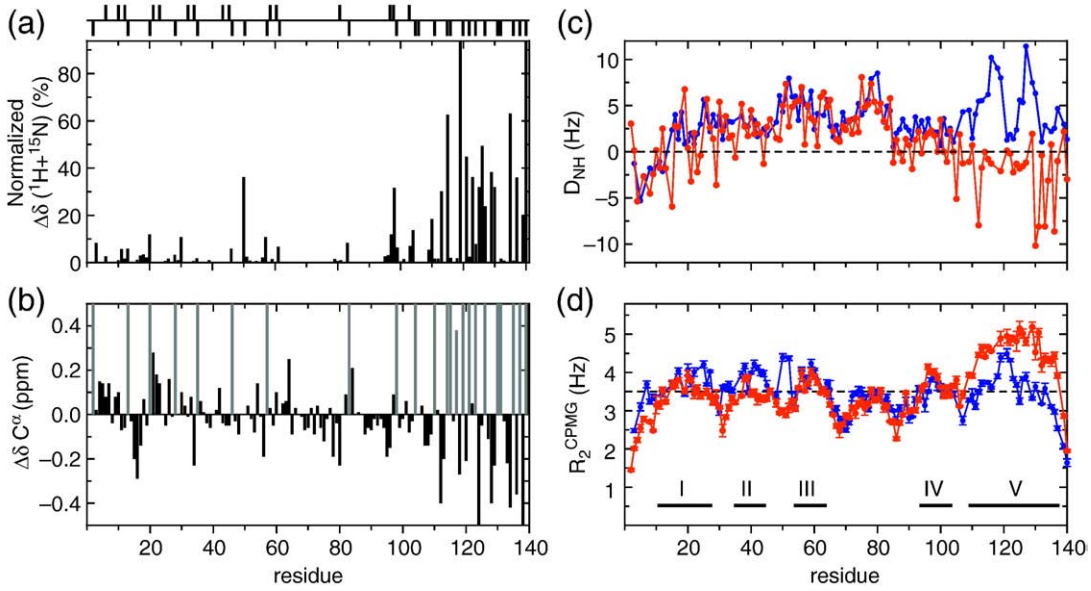

Fig. 2. NMR parameters for α-synuclein at neutral and low pH. Distribution of charged residues shown in Fig. 1 is displayed at the top of the figure. Comparison of chemical shifts (a and b), RDC (c), and R_2^{CPMG} (d) data of α-synuclein at acidic and neutral pH. (a) Average differences of H^{N} and ^{15}N chemical shifts at pH 2.5 and 7.4 with the formula $\Delta\delta = \sqrt{\{[(\Delta H^{N})^2 + 0.2(\Delta^{15}N)^2)]/2\}}$ and the values are normalized. (b) C^{α} chemical shift differences between pH 7.4 and 2.5 ($\Delta\delta C^{\alpha} = \delta C^{\alpha}_{7.4} - \delta C^{\alpha}_{2.5}$) are shown. Asp and Glu residues are colored light gray. (c) ^{1}H–H^{N} RDCs at pH 2.5 and 7.4 are shown in red and blue lines with dots, respectively. (d) R_2^{CPMG} relaxation rates at pH 2.5 and 6.1 are displayed with red and blue lines with dots, respectively. Average value (3.5 Hz) of R_2^{CPMG} at pH 2.5 is indicated. Regions of five defined segments are shown in bars and numbered.

cally disordered at pH 2.5. Backbone assignments were carried out based on ^{15}N–^{15}N connections using the 3D HNN triple-resonance experiments.[41] Out of 140 residues, 134 (no Met[1] and 5 prolines) were assigned in the ^{1}H–^{15}N HSQC spectrum and most of the ^{1}H and ^{15}N chemical shift changes arise in the C-terminal region of the protein (Fig. 2a) where there are 3 Asp and 12 Glu residues. The major changes in C^{α} shifts ($\Delta\delta C^{\alpha}$, Fig. 2b) from pH 7.4 to pH 2.5 can be directly tied to the protonation of Asp and Glu residues at low pH. Once those changes are accounted for, the remaining small $\Delta\delta C^{\alpha}$'s in the N-terminus and NAC regions alternate between positive and negative values, indicating that the secondary-structure propensities are essentially the same at low and neutral pH. There is, however, a stretch of small negative values in the C-terminus region, which represents a small decrease in the β propensity in this region of the protein at low pH.

Residual dipolar coupling (RDC) constants have been employed to probe the local structural ordering[42,43] as well as long-range contacts[30,44] of IDPs. We have measured the D_{NH} values of α-synuclein at pH 7.4 and pH 2.5 using an *n*-alkyl-poly(ethylene glycol)/*n*-alkyl alcohol mixture [pentaethylene glycol monooctyl ether (C8E5)/1-octanol] as the alignment medium. Significant differences can be seen in the RDC profiles at pH 7.4 and pH 2.5, particularly at the C-terminus and the leading portion of the N-terminus (Fig. 2c). At pH 2.5, the D_{NH} values are close to zero or negative at residues 100–127 and even more negative (~−8 to −10 Hz) at the end of the C-terminus. The D_{NH} values in the NAC region and the N-terminal region are similar to the D_{NH} values measured at pH 7.4, indicating that these regions are relatively insensitive to the environmental changes.

^{15}N backbone transverse relaxation experiments using the CPMG pulse train (R_2^{CPMG}) indicate that the low-pH and near-neutral-pH forms of α-synuclein exhibit different local dynamics along the sequence (Fig. 2d). We have compared the R_2^{CPMG} experiments at pH 2.5 and pH 6.1 rather than pH 7.4 as we have shown (unpublished data) that the intrinsic R_2^{CPMG} values at pH 7.4 are modulated by the fast hydrogen exchange rates that exist at this pH. A more accurate view of the intrinsic R_2^{CPMG} values can be obtained at pH 6.1 where the hydrogen exchange rates are slower. The R_2^{CPMG} values can be classified into five segments (10–25, 32–42, 52–62, 93–105, and 109–136) using R_2^{CPMG}=3.0 Hz as cutoff. The overall features of the R_2^{CPMG} data are similar for the two pH values with the exception of the C-terminal end from residues 105 to the end of the protein. Here, the R_2^{CPMG} values are uniformly greater at low pH than at neutral pH, suggesting that the C-terminal end of the protein is experiencing restricted motion and is more rigid at low pH. In the NAC region, for both pH values, the R_2^{CPMG} values are the smallest, indicating that this region is the most flexible.

The C-terminus is collapsed at pH 2.5

Site-directed spin labeling and PRE at three positions, A19, A90 and G132, are used to obtain information about long-range interactions within the unfolded protein. The PRE effects are compared at pH 7.4 and pH 2.5 and show differences, especially in terms of the interactions observed at the C-terminal end of the protein. At pH 7.4 (Fig. 3a), the

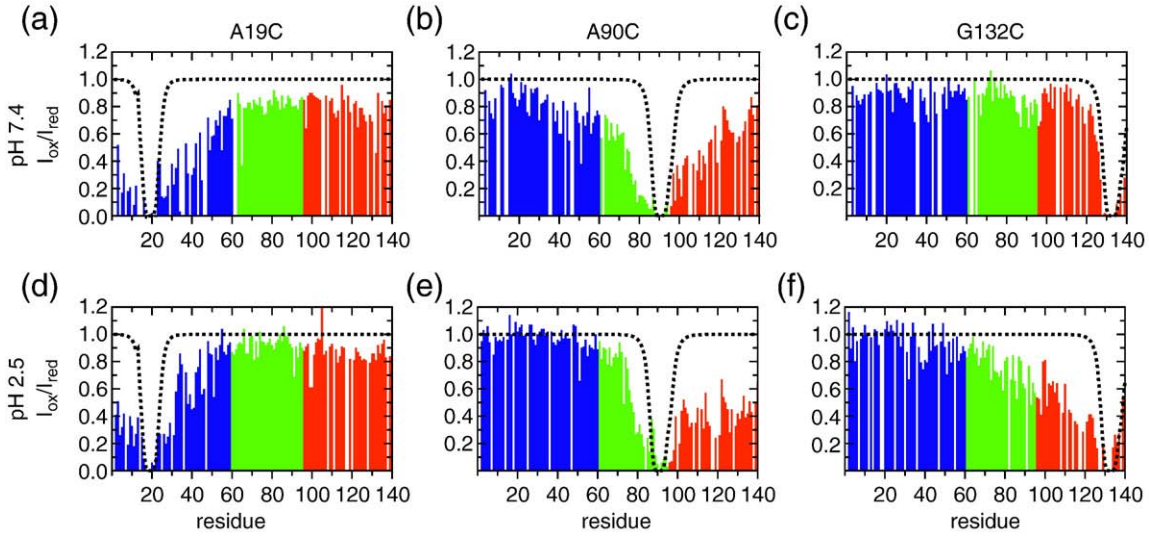

Fig. 3. PRE intensity ratios for spin-labeled α-synuclein. Paramagnetic relaxation experiments of amide protons in human α-synuclein at pH 7.4 (a–c) and pH 2.5 (d–f) using MTSL spin labels for cysteine mutants A19C, A90C, and G132C. Measured PRE intensity ratios (I_{ox}/I_{red}) are presented in the top (pH 7.4) and bottom (pH 2.5) panels. White gaps in each plot are unassignable residues including five prolines. N-terminal, NAC, and C-terminal regions are colored blue, green, and red, respectively. Broken lines are the theoretical PRE values of α-synuclein without any long-range contacts calculated as described previously.[29]

spin label at A19C results in diminished intensity throughout the entire sequence with a maximum observed value of $I_{ox}/I_{red} \sim 0.8$. At the N-terminus, there is a slow increase in I_{ox}/I_{red} up to residue 60, at which point the intensity plateaus at ~0.8. The same spin label at pH 2.5 (Fig. 3d) has a progressively faster increase in PRE intensity at the N-terminus and plateaus at a higher level close to 1.0 in the NAC region and C-terminal to it. There is a small reduction in intensity ($I_{ox}/I_{red} \sim 0.8$) at the very end of the C-terminus from residues 110 to 140. At neutral pH, there are numerous short-range contacts between residue 19 and the N-terminus as well as transient contacts between residue 19 and the NAC and C-terminal regions consistent with previous experimental results.[23,30] At low pH, the N-terminal region has fewer interactions with the N-terminal spin label and the NAC region is not interacting with the N-terminal spin label and is only making very local transient contact at a small region of the C-terminus (residues 115–130).

The PRE results at A90C in the NAC region (Fig. 3b and e) show distinct features at neutral and low pH. At pH 7.4, the PRE I_{ox}/I_{red} pattern is similar to the published data obtained by placing the PRE label at position A85[28] or A90.[30] The A90C spin label probe at pH 7.4 interacts primarily with the second half of the N-terminal region (40–60) as well as with the C-terminal region. In contrast, at pH 2.5, there are essentially no interactions with the N-terminal region and increased interactions with the C-terminal region ($I_{ox}/I_{red} = 0.4–0.6$) relative to the neutral pH.

The spin label at position G132C (Fig. 3c and f) has a very different intensity profile at neutral and low pH in particular in the C-terminal region of the protein. At neutral pH, the spin label does not lead to strong signal attenuation anywhere in the sequence. Three small dips in the intensity ratio ($I_{ox}/I_{red} = \sim 0.8$) are observed, one in the NAC region from residues 80 to 100 and two in the N-terminus, around residues 30–40 and near residue 5. This profile has similar trends to those seen by Bertoncini *et al.*[30] and Sung and Eliezer[23] who have studied the effects of spin labels at positions A140C and P120C, respectively; however, the decrease in the intensity ratio is somewhat smaller for the data observed here with the spin label at position 132. The PRE effects due to the G132C spin label at low pH (Fig. 3f) are quite different; there is no signal attenuation in the N-terminus, but there is strong signal attenuation in the C-terminus ($I_{ox}/I_{red} \sim 0.4$), which continues, gradually weakening (I_{ox}/I_{red} goes from 0.4 to 0.9), into the NAC region. The weak signal attenuation from G132C at neutral pH suggests that the protein is making infrequent transient C- to N-terminal contacts. However, at pH 2.5, the PRE profile shows a cluster of long-range contacts between the C-terminal spin label and the C-terminal end and NAC region.

Pulsed-field gradient NMR (PFG-NMR) translational diffusion experiments were performed at low and neutral pH in order to obtain the effective hydrodynamic radius (R_h) of the proteins. The R_h value at 15 °C and pH 2.5 ($R_h = 30.1$ Å) is smaller than that at pH 7.4 ($R_h = 31.7$ Å), suggesting that low pH induces a conformational compaction relative to the neutral pH value. Uversky *et al.* have also observed a compaction at low pH relative to neutral pH;[31] they saw a decrease in the radius of gyration from 40 Å at pH 7.5 to 30 Å at pH 3.0. The large gap in the radius of gyration values relative to the hydrodynamic radii is because the radius of gyration, which measures the average distance of each residue from the center of mass of the protein, is more sensitive to the extension of the chain than the

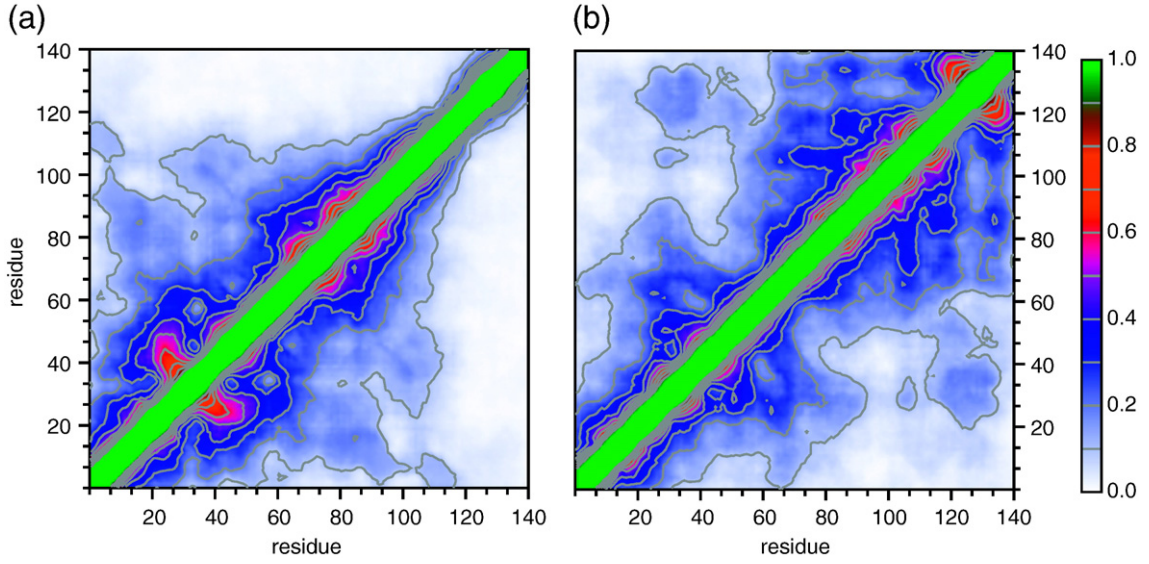

Fig. 4. REMD simulation results exhibit good agreement with experimental data. Contact maps of α-synuclein ensembles at neutral pH (a) and low pH (b) calculated using REMD. The color gradient from white, to blue, to red, to green represents percentages of the conformational ensembles that have inter-residue C^{α}–C^{α} distances within 20 Å.

hydrodynamic radius, which approximates the radius of a sphere whose diffusion constant equals that of the protein.[45]

Visualization of the conformational ensemble of α-synuclein by REMD at low pH

Replica exchange molecular dynamics (REMD) simulations were employed to generate conformational ensembles of α-synuclein at neutral and low pH. Long-range contacts within the neutral- and low-pH ensembles are consistent with the long-range contacts observed experimentally through PRE measurements. Figure 4 shows the percentage of the population within the low- and neutral-pH ensembles with inter-residue contacts (C^{α}–C^{α} distances) within 20 Å. A cutoff of 20 Å was chosen to facilitate comparison with experimental PRE measurements, which can detect contacts within 20–25 Å of the nitroxide spin label. At neutral pH (Fig. 4a), there are contacts observed throughout the N-terminus and NAC regions, while the C-terminal tail (residues 115–140) is largely extended, making contact with the other regions in only ~5% of the population. In the contact map for the low-pH ensemble (Fig. 4b), the region of the protein that shows many intramolecular contacts has switched relative to the neutral-pH ensemble. At low pH, the C-terminus is in regular contact with itself and the NAC region, as well as a small section of the N-terminus near residue 40, but only approaches the most N-terminal part of the protein in a small fraction of the population. The section of the N-terminus near residue 40 makes transient contact not only with the C-terminus but also with the N-terminal half of the NAC. However, the leading portion of the N-terminus, from residues 1 to 40, forms a separate cluster of long-range contacts and has fewer contacts with the rest of the protein. The switch from an extended C-terminus at neutral pH to a somewhat less extended N-terminus at low pH is also seen in calculations of the solvent-accessible surface area (SASA) (Fig. 5a). The C-terminus at neutral pH has the highest solvent accessibility (75.4%) of any region at either pH. However, at low pH, the N-terminus is the region most exposed to the solvent (68.6%), while the NAC and C-terminus have an equal amount of solvent accessibility (59%). Interestingly, the NAC solvent exposure is very similar at both neutral and low pH. It appears that the NAC region "swaps" intermolecular contacts with the N-terminal region at neutral pH for corresponding contacts with the C-terminal residues at low pH.

Simulated PRE intensity ratios for the neutral- and low-pH conformational ensembles (Fig. S1) portray the same trends seen in the contact maps. At neutral pH, the intensity ratio profiles show significant contacts between the N-terminus and NAC regions, while the C-terminal spin label site is only in contact with the rest of the sequence in a very small percentage of the population. Interestingly, the simulated ensemble does show a dip in the intensity ratio from

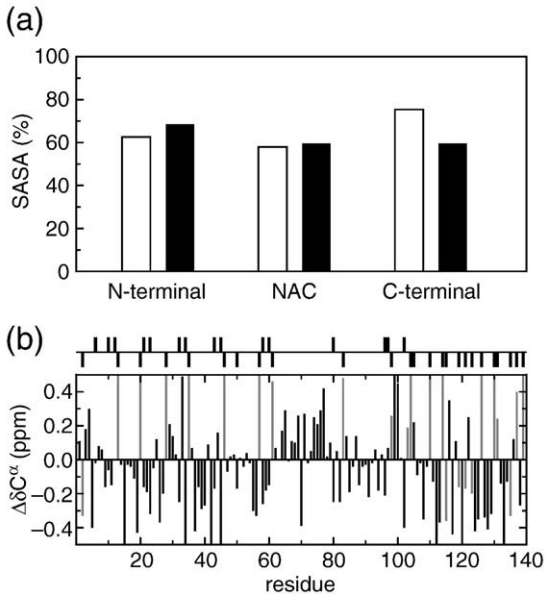

Fig. 5. SASAs at neutral and low pH. (a) Comparison of percentage of SASAs for the N-terminal, NAC, and C-terminal regions of the neutral (open bars) and low (filled bars) pH ensembles. A significant change in the solvent accessibility is observed in the C-terminal region, which is less exposed, supporting the idea of a collapsed conformation in this region. (b) Calculated differences in average chemical shifts between the low- and neutral-pH ensembles ($C^{\alpha}_{neutral} - C^{\alpha}_{low}$). Asp and Glu residues are colored light gray. The chemical shifts were calculated using ShiftX.[46]

G132C in the N-terminus near residue 10. At low pH, the calculated PRE profiles are consistent with fewer contacts between the N-terminus and the NAC but show very significant drops in the intensity ratio in the C-terminus from the A90C spin label and in the NAC from the G132C spin label. Overall, the calculated intensity ratio profiles, such as the contact maps, exhibit large changes in the C-terminus when going from neutral to low pH and smaller changes in the N-terminus.

The inter-residue contact maps (Fig. 4a and b) provide information about the long-range contacts of the ensemble. Local structural characteristics, particularly secondary-structure propensities, are often related to chemical shifts that are affected by the local environment of the nucleus being monitored.[24,47] We calculated the C^{α} chemical shifts for the low- and neutral-pH ensembles. There are large changes in C^{α} ($\Delta\delta C^{\alpha}$, Fig. 5b) that can be attributed to the change in the charge state of the Asp and Glu residues, just as with the experimental C^{α} measurements. However, even accounting for the protonation of the negatively charged residues, there are more differences in the C^{α} shifts of the simulation ensembles than are observed experimentally. The calculated $\Delta\delta C^{\alpha}$'s show that the biggest chemical shift difference is in the C-terminal region and that it not only corresponds to decreased β, similar to the experimental observation, but also features stretches

Table 2. Compaction ratios of REMD-simulated ensemble of α-synuclein

pH	N	NAC	C
Neutral	0.55	0.5	0.81
Low	0.63	0.56	0.52

The table shows the compaction ratios of the N, NAC, and C regions for the low-pH and neutral-pH α-synuclein simulation ensembles, calculated as the ratio of average end-to-end distance in the low (or neutral) pH ensemble to the same quantity for the denatured state ensemble.

of negative $\Delta\delta C^{\alpha}$ in the N-terminus and positive $\Delta\delta C^{\alpha}$ in the NAC region, indicative of decreased β propensity and decreased α propensity, respectively. The overall β structure of the ensembles, as calculated by STRIDE,[48] decreases as the pH is lowered, consistent with the trend predicted by the experimental $\Delta\delta C^{\alpha}$ measurement. There is no significant helical structure observed for either simulated ensemble. Though there is slightly more variation in the chemical shifts of the simulated ensembles compared to the experiments, in both cases, the largest differences are found in the C-terminus and the magnitude of the chemical shift differences throughout the sequence is very small. This suggests that there is little difference in secondary-structure propensity at neutral and low pH, with the biggest change being a slight decrease in β propensity in the C-terminus at low pH.

Relative packing of the N-terminal, NAC, and C-terminal regions of α-synuclein was evaluated by determining compaction ratios (see Materials and Methods). The values (Table 2) are consistent with the picture provided by the contact maps. At neutral pH, the N-terminus and NAC regions have similar compaction ratios, 0.55 and 0.5, respectively, but the C-terminus is much more expanded, with a compaction ratio of 0.81. In contrast, at low pH, the C-terminus has a compaction ratio similar to that of the NAC, 0.52 and 0.56, respectively, while the N-terminus is more expanded, with a compaction ratio of 0.63. Here, again, the region most affected by the change in pH is the C-terminus, whose compaction at low pH is reflected in the change of the compaction ratio from 0.81 to 0.52.

Molecular simulations allow for the visualization of individual structures within the conformational ensembles. We used a clustering algorithm[49] to select structures from the REMD simulations. The conformations from the neutral-pH ensemble shown in Fig. 6a were chosen from the top four clusters, representing more than 53% of the ensemble. The representative structures from the low-pH ensemble (Fig. 6b), chosen from the top three clusters and representing more than 60% of the total population, provide the first visualization of structures from an ensemble consistent with experimental observations at low pH. These figures highlight the structural changes at low pH relative to neutral pH previously observed in both the PRE measurements and the contact maps for the simulation ensembles, namely, the compaction of the C-terminal region at low pH coupled with an N-terminal region, which is less extended than the C-terminus at neutral pH.

Discussion

We have used two approaches, NMR spectroscopy and computer simulation, to characterize the conformational ensembles of the IDP α-synuclein at both neutral and low pH. By NMR, we have measured

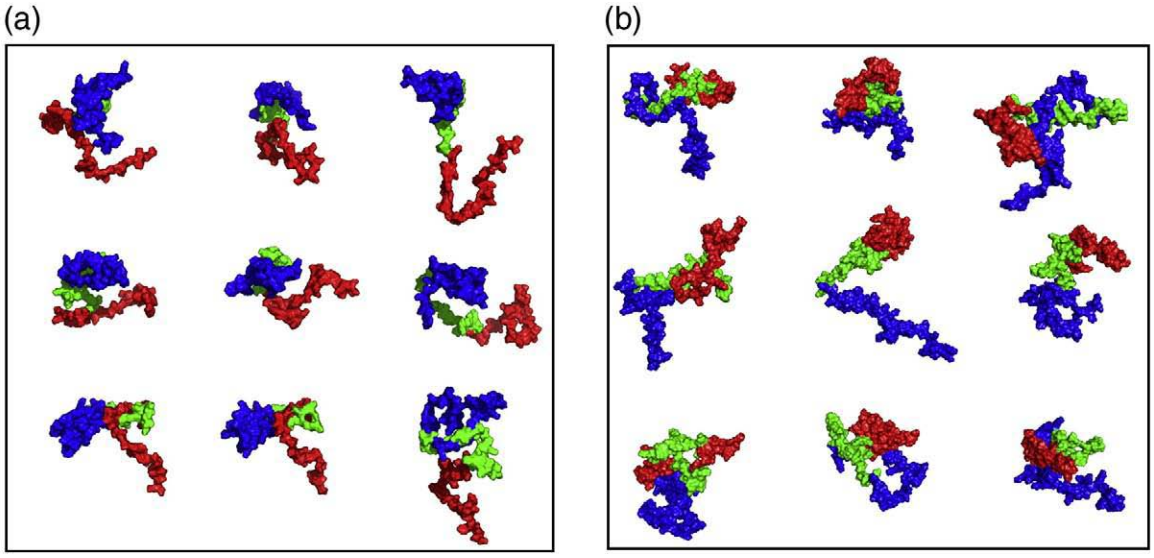

Fig. 6. Selected representative conformations of α-synuclein from the neutral-pH and low-pH ensembles. Representative structures chosen from (a) the top four clusters of the neutral-pH ensemble and (b) the top three clusters from the low-pH ensemble. These clusters account for more than 53% and 60% of the respective structural ensembles. The N-terminus is shown in blue, the NAC is shown in green, and the C-terminus is shown in red.

chemical shifts, RDCs, R_2^{CPMG}, and PREs of α-synuclein at pH 7.4 and 2.5 in order to compare the secondary structure and long-range interactions within the protein and to explore differences in dynamics. We have also used REMD with implicit solvent to simulate α-synuclein at neutral and low pH. The simulations allow us to visualize the conformational ensembles at low pH and compare these directly to the conformations populated at neutral pH.

α-Synuclein at neutral pH has been extensively studied by NMR.[15,29,30,32] Our experimental measurements at pH 7.4 reproduce the same general features observed in previous studies. The effect of the N-terminal spin label is seen throughout the remainder of the N-terminus and results in a small, uniform reduction in the intensity ratio in both the NAC and the C-terminus. We interpret the uniformly reduced intensity ratio throughout the NAC and C-terminus as a consequence of transient contacts between A19C and each residue from 60 to 140; it is a reflection of the heterogeneity of the structural ensemble since it implies that A19C is not involved in unique, long-range contacts with any particular residues in the C-terminal part of the protein. An alternative explanation for the plateau is that there is a scaling problem between the oxidized and reduced experiments that lowers the baseline but is not indicative of any actual contact between A19C and the residues of the NAC and C-terminal regions. However, the fact that a similar effect is seen in the PRE intensity ratios calculated from the REMD ensembles (Fig. S1) lends credibility to the observed results, since there can be no question of a scaling problem in the simulations. The neutral-pH conformational ensemble generated by the simulations qualitatively portrays the same long-range interactions observed by the NMR experiments. Intermittent contacts between the N-terminus and the other regions of the protein are seen both in the contact maps and in the calculated PRE intensity ratios. Moreover, in both the experimental and the calculated PRE plots, the C-terminal probe at G132C induces very little reduction in intensity from the line corresponding to the intensity ratio expected for a random coil, except for a small dip in the N-terminus near residue 20. This suggests that with the exception of a small population of conformations in which the N- and C-termini are in contact, the C-terminus is largely extended into solution.

While our analysis of the neutral-pH REMD ensemble suggests that it qualitatively captures the long-range interactions observed experimentally, it is quite different from the ensemble previously obtained by Bertoncini *et al.*[30] In their study, agreement with experiments was enforced through the use of PRE-derived distance constraints. The structures they show, representatives of seven clusters accounting for more than 50% of their conformational ensemble, are all shaped like rings, with the N- and C-termini in contact with each other. That two such different ensembles can be obtained, which both appear to agree with PRE data, is a reflection of the fact that the determination of structural ensembles from PRE data is a very underdetermined problem.[50] PRE intensities are related to the distance between each residue and the nitroxide spin label via a $1/r^6$ average over the conformational ensemble. As a consequence of this $1/r^6$ distance dependence, PRE intensities are dominated by contributions from more compact conformations. Small changes in the population of conformations containing residues a short distance from the spin label will have a big effect on the $1/r^6$ average; this decreases the constraints on other conformers and can allow for the inclusion of large populations of expanded conformations in an ensemble matching a given PRE intensity ratio profile. This means that the distances derived from the spin labels attached to the protein in PRE experiments can be satisfied by many different conformational ensembles. It has recently been demonstrated that if it were experimentally feasible to attach many more spin labels, covering a large percentage of the protein, then there would be enough data generated to be able to uniquely identify the true conformational ensemble.[50]

NMR experiments and REMD simulations indicate that there is a significant structural reorganization within the low-pH ensemble relative to that at neutral pH in terms of long-range contacts, hydrodynamic radius, and the amount of heterogeneity within the conformational ensembles. The rearrangement of long-range contacts is observed by comparing the PRE measurements and REMD contact maps at low pH with the corresponding descriptions of the neutral-pH ensemble. Both the PREs and the contact maps show that the largest change takes place in the C-terminus. Whereas the C-terminal region in the neutral-pH ensemble is largely extended, only making contact with the other regions transiently, at low pH, there are numerous contacts between the C-terminus and the tailing portion of the NAC (Fig. 3e and f). The C-terminus at low pH is also more compact, has decreased flexibility based on ^{15}N relaxation data, and is less exposed to the solvent than at neutral pH. The response of the N-terminal region to the change in pH is less dramatic. While the N-terminus at low pH is both more extended and more exposed to solvent than at neutral pH, neither of these changes are as large as those observed in the C-terminus. These results highlight the change in the long-range interactions between the neutral- and low-pH ensembles; at neutral pH, there is a very heterogeneous ensemble with transient contacts between the N-terminus and the NAC; however, at low pH, there is a more homogeneous ensemble that exhibits strong contacts between the NAC and the C-terminus. Transient contacts between the N- and C-termini are observed at both pH values.

NMR experiments and REMD simulations show that the low-pH ensemble of α-synuclein has a smaller average hydrodynamic radius than the neutral-pH ensemble. From the experimental data and the visualization of the REMD structures, it is clear that there is no global collapse of the protein at

low pH but rather the compaction is local and exists primarily in the C-terminal domain and the C-terminal region of the NAC. Uversky *et al.* have proposed, based on CD and Fourier transform infrared spectroscopy measurements, that the low-pH form of α-synuclein has increased β content relative to the neutral-pH form, a relatively compact conformation, and can be thought of as a pre-molten globule state.[31] The detailed atomic description presented here indicates that the compaction is primarily restricted to the last 60 residues of the protein and that the N-terminal region is more exposed. In addition, there is no evidence at the individual residue level of an increase in β conformation in the low-pH ensemble relative to the neutral-pH ensemble.

The structural reorganization at low pH can be rationalized by considering the distribution of charges that exist in the low-pH form relative to the neutral-pH form. As seen in the charge density table (Table 1), the three regions of α-synuclein are impacted differently by lowering the pH. In particular, there is a large change in the total charge density in the C-terminus that decreases from 40% charged residues at neutral pH to only 6.7% charged residues at low pH. In contrast, the effect of low pH on the N-terminus is less pronounced with a shift from 30% charged residues at neutral pH to 18.3% charged residues at low pH and a total charge that is high at both pH values. Overall, the decrease in the total charge density of the C-terminus is considerably more than the change at the N-terminus and accounts for the fact that the reorganization of the C-terminus is the most pronounced and that of the N-terminus less so.

Uversky *et al.* have empirically observed that IDPs and globular proteins fall into two distinct regions as a function of their mean net hydrophobicity *versus* mean net charge.[51] They noted that in the plot of hydrophobicity *versus* charge, α-synuclein is one of the few examples of an IDP that is just over the line into the ordered region of the plot (Fig. 7). However, we consider the three functional regions of α-synuclein separately and note that the C-terminal region at neutral pH, with a net charge of −12, resides very definitively in the IDP region of the Uversky plot. At low pH, however, the C-terminus loses most of its net charge and becomes highly hydrophobic. The very dramatic movement of the C-terminus to the ordered region may be due to the high density of glutamates in the sequence that become very hydrophobic at low pH. The globular-like quality of the C-terminus that is predicted in the plot is reflected in the NMR experiments and REMD calculations where the C-terminal compaction is seen both in the experimental PRE measurements and the contact map of the simulated low-pH ensemble. The full α-synuclein sequence at low pH moves more fully into the ordered region of the charge *versus* hydrophobicity plot due to an increase in hydrophobicity. This shift is mirrored by the smaller hydrodynamic radius observed at low pH. Interestingly, because of the balance between

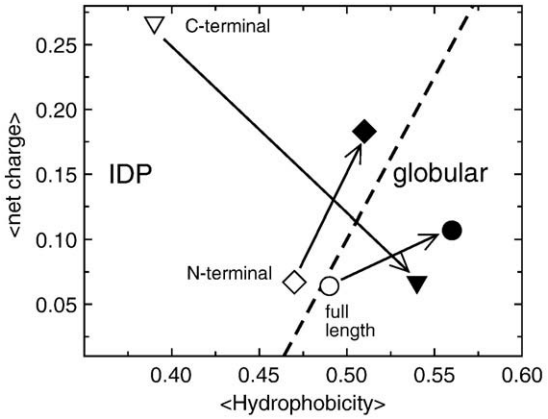

Fig. 7. Charge-hydrophobicity characteristics of α-synuclein. Charge-hydrophobicity characteristics of α-synuclein at low (filled symbols) and neutral (open symbols) pH. The hydrophobicity values for α-synuclein were calculated using the Cowan–Whittaker hydropathy indices[52] for the low- and neutral-pH conditions using a window size of five amino acids. The hydrophobicity values for the individual amino acids were normalized to a 0-to-1 scale. The mean net hydrophobicity (net charge) was calculated as the sum of normalized hydrophobicity (charge at specific pH) divided by the total number of residues in α-synuclein. The black line represents the boundary between globular proteins and IDPs determined using a list of these proteins, an analysis similar to that performed by Uversky *et al.*[51]

positively and negatively charged residues in the N-terminus at neutral pH, the N-terminus has both a higher net charge and a slightly higher net hydrophobicity at low pH and remains in the IDP region of the plot.

α-Synuclein has been shown to aggregate more rapidly at low pH, and a comparison of the structural and dynamical differences may aid in understanding which factors are critical to aggregation. Aggregation may be affected by a number of properties including propensity to form transient secondary structure,[23] the distribution of long-range interactions,[30,32] the hydrodynamic radius of the protein,[31] the flexibility of different regions and their exposure to solvent,[29,53] and the distribution of charges along the protein.[54] We find that the C^{α} chemical shifts of the neutral- and low-pH forms are quite similar, and this suggests that secondary-structure propensity is not a driving force to increase the aggregation rate at low pH. It has previously been suggested that the increased rates of aggregation observed for single point mutations[25] or upon binding of divalent metal ions[55] or polycations[30,56] are due to the release of the long-range N- to C-terminal contacts and subsequent exposure of the NAC. However, the results of the REMD simulations suggest that the NAC region has comparable exposure to solvent at both neutral and low pH; NMR R_2^{CPMG} measurements suggest that the NAC region has comparable flexibility in both pH forms. Similar exposure of the NAC region to solvent in both the slower, neutral-pH and faster, low-pH aggregating species suggests that protection or

exposure of the NAC region may not have a large impact on the aggregation propensity in this context.

At low pH, where the charge profiles of both the N- and C-termini are significantly different from their neutral-pH counterparts, it is possible that initiation of aggregation may arise through a different mechanism. Previously, we proposed for mouse α-synuclein at neutral pH that aggregation may be initiated through intermolecular N-terminal contacts. While the N-terminus has a balance of positively and negatively charged residues at neutral pH in both mouse and human α-synuclein, it carries a large positive charge at low pH. Without complementary negative charges anywhere in the sequence, it may be reasonable to assume that the N-terminus is unlikely to initiate intermolecular contacts at low pH. One scenario that is consistent with the structural changes and charge distribution at low pH is that the locally collapsed C-terminus, which loses its net charge and becomes highly hydrophobic under these conditions, is involved in the earliest stages of α-synuclein aggregation at low pH. These data indicate the importance of the charge distribution in directing both the mechanism and the rates of aggregation.[54]

Materials and Methods

Sample preparation

Expression and purification of human α-synuclein in *Escherichia coli* were followed by the described protocol.[29] Further purification using diethylaminoethyl or Q anion-exchange chromatography was applied to ensure high purity of α-synuclein for low-pH studies. α-Synuclein was eluted at 200–300 mM NaCl gradient. Solution containing pure α-synuclein was dialyzed against with 20 volumetric times of phosphate-buffered saline (PBS; pH 7.4) at 4 °C and repeated 3 times. Dialyzed and concentrated α-synuclein (200 μM) was transferred to 1.5-ml tubes and quickly frozen by cryogenic liquid nitrogen for −80 °C storage. For each NMR sample, the −80 °C stored proteins were unfrozen at 4 °C, polished using a 100-kDa filter (Millipore), and then dialyzed to pH 2.5 (10 mM phosphate and 140 mM NaCl) with the addition of 10% D_2O.

NMR experiments for assignment

NMR experiments including triple-resonance experiments and ^{15}N backbone dynamics experiments were performed on a Varian 800-MHz spectrometer equipped with triple gradient probe. PFG-NMR diffusion, PRE and RDC measurements were acquired on a Varian 600-MHz spectrometer with a cold probe or on a Bruker 700-MHz spectrometer. Acquired spectra were processed by NMRPipe[57] and analyzed by Sparky.[58]

^{13}C–^{15}N-labeled α-synuclein (650 μM) at pH 2.5 was used to perform triple-resonance experiments for backbone assignment at 15 °C. The 3D spectra were acquired via the conventional strategy[59] using HNCACB, CBCA(CO)NH, HNCO, and HN(CA)CO and a new approach using HNN[41] via ^{15}N–^{15}N connections. Data collection time for each 3D spectrum at 15 °C is shorter than 20 h (with 8 or 16 transient scans) to avoid aggregation during acquisition. HSQC spectra were collected to check the stability of α-synuclein before acquiring the next 3D spectrum.

Chemical shifts were calibrated using 2,2-dimethyl-2-silapentane-5-sulfonate dissolved at pH 2.5 as a reference.[60] Comparing the secondary-structure propensity using the C^α chemical shift deviation from the random-coil shifts is not appropriate since the random-coil C^α chemical shifts measured at pH 5.0[61] and 2.3[62,63] exhibit significant differences. Directly monitoring the changes of C^α chemical shifts ($\Delta\delta C^\alpha = \delta C^\alpha_{7.4} - \delta C^\alpha_{2.5}$) was used to inspect the secondary-structure propensities at pH 7.4 and 2.5.

Translational diffusion coefficients and hydrodynamic radii

PFG-NMR experiments incorporated with longitudinal eddy current pulse schemes and convection compensation were used to measure the translational diffusion coefficients (D_{trans}).[64] Samples containing 300 μM α-synuclein and 35 mM 1,4-dioxane were dissolved in PBS buffers at pH 7.4 and 2.5 (100% D_2O, pD uncorrected) for PFG-NMR experiments at 15 °C. Twenty-five 1D PFG-NMR spectra were acquired over a range of gradient strengths of 2 to 17 G/cm or 5 to 50 G/cm for 1,4-dioxane or α-synuclein, respectively. Integrated peak volumes of 1,4-dioxane and α-synuclein (methyl groups only) were fitted using VNMRJ 2.1 (Varian Inc., California) and used to calculate D_{trans}.[64] Since α-synuclein and dioxane were dissolved in one solution, the viscosity effect on D_{trans} can be ignored. Therefore, the Stokes–Einstein equation can be simplified to get the hydrodynamic radius of α-synuclein by the relationship:

$$R_h(\alpha - \text{synuclein}) \times D_{trans}(\alpha - \text{synuclein}) = R_h(\text{dioxane}) \times D_{trans}(\text{dioxane})$$

where R_h (dioxane) is 2.12 Å.

^{15}N relaxation

R_2^{CPMG} ^{15}N relaxation experiments were acquired using 250 μM ^{15}N-labeled α-synuclein at pH 2.5 and 6.1. Complex points for each spectrum were 1024×256 in the ^1H and ^{15}N dimensions, respectively. The relaxation times for R_2^{CPMG} were 0.01, 0.03, 0.05, 0.09, 0.13, 0.17, 0.19, 0.21, and 0.25 s. Recycle delays for each experiment were 2 s. Data were processed by NMRPipe and analyzed by Sparky.

Site-directed spin label

Methods for (1-oxy-2,2,5,5-tetra-methyl-3-pyrroline-3-methyl)-methanesulfonate (MTSL) (Toronto Research Chemicals, Ontario, Canada) spin-labeled ^{15}N-α-synuclein A19C, A90C, or G132C were done as described in our previous work.[29] In brief, 250 μM MTSL-labeled α-synuclein cysteine mutants were dialyzed to pH 2.5 or 7.4 and were divided to equal volume for experiments at paramagnetic (oxidized) and diamagnetic (reduced) states. Addition of 10 mM L-ascorbate (pH 2.5) or 10 mM dithiothreitol (DTT) (pH 7.4) was applied for generating the diamagnetic samples. It is not possible to use DTT or L-ascorbate as a reducing reagent at both pH values. DTT cannot be used at low pH as the disulfide bond is not efficiently broken at pH 2.5 because the thiol groups are

highly protonated. At neutral pH, we have observed significant signal enhancements and changes of ^{1}H and ^{15}N chemical shifts in the presence of L-ascorbate. PRE ratios (I_{ox}/I_{red}) were calculated as the intensity ratios of the same residue in the absence (I_{ox}) or in the presence (I_{red}) of L-ascorbate or DTT. At low pH, all mutant samples were normalized against L-ascorbate, and at neutral pH, all samples were normalized against DTT.

RDC measurement

n-Alkyl-poly(ethylene glycol)/*n*-alkyl alcohol mixture[65] was chosen to prepare the liquid crystalline medium for RDC experiments; 5% C8E5 and 1-octanol were mixed with PBS buffer at pH 2.5 or 7.4. The molar ratio of C8E5 and 1-octanol is 1.05. The quadrupolar deuterium splitting constants are 23.8 and 22.7 Hz at pH 7.4 and 2.5, respectively. High-resolution HSQC_IPAP spectra in the absence or in the presence of an alignment medium were collected at 15 °C with complex points of 2048 (t_2) × 512 (t_1) and 16 transient scans.

REMD simulations

REMD[66,67] simulations were used to generate the conformational ensembles of α-synuclein at low and neutral pH. In this method, a number of simulations (replicas) are run in parallel over a specified temperature range. The adjacent replicas (T_i and T_j) are allowed to exchange periodically, with an acceptance criterion based on the following Metropolis transition probability:

$$W\{T_i, T_j\} \rightarrow \{T_j, T_i\} = \min\left(1, \exp\left[-\left(\beta_j - \beta_i\right)\left(E_j - E_i\right)\right]\right)$$

where $\beta_{i(j)} = 1/KT_{i(j)}$ and $E_{i(j)}$ is the potential energy of the *i*th (*j*th) replica. This method provides canonical probability distributions for the ensembles over the specified temperature range.[67] The REMD method has been implemented in the IMPACT simulation package.[68] The simulations were performed using the AGBNP implicit solvent[69] model and the OPLS-AA force field.[70]

The simulation was performed for a total of 10 ns over 20 temperatures (300, 308, 317, 325, 334, 343, 353, 362, 372, 382, 393, 403, 414, 426, 437, 449, 461, 474, 487, and 500 K), corresponding to a total simulation time of 200 ns. All simulations were started with a fully extended conformation of the α-synuclein molecule. The sequence of α-synuclein, for the low-pH condition, was modified to a state corresponding to that of the molecule under these conditions, by protonating the side-chain carbonyl groups of all of the acidic residues (aspartates and glutamates). α-Synuclein was also simulated with a purely repulsive potential, in which all interactions have been turned off except for the repulsive part of the Lennard–Jones potential, to obtain the ensemble of structures corresponding to the denatured or most expanded state. The 449 and 414 K ensembles were used for the structural characterization of the low- and neutral-pH ensembles. These ensembles were chosen because their hydrodynamic radii (29.1 and 30.5 Å, respectively) most closely matched the experimental measurements at 15 °C.

A number of analysis methods were used for the structural characterization of the low-pH ensembles. The average size of the ensembles was determined by calculating the hydrodynamic radii for individual structures using Hydropro.[71] The secondary structural assignments for the α-synuclein ensembles were made using STRIDE.[48] C^{α} chemical shifts were calculated using ShiftX.[46] The SASAs were calculated using the program Surfv.[72] The clustering of the neutral- and low-pH ensemble structures was performed using a hierarchical clustering method,[49] with the clustering based on a distance matrix of distances between the center of mass of the three regions of synuclein (N-terminus, NAC, and C-terminus). The compaction factors for the low- and neutral-pH conditions were calculated as the ratio of the average end-to-end distance between the low (neutral) pH and the denatured state of α-synuclein. The end-to-end distance of the denatured state was calculated from an ensemble generated using a purely repulsive potential, which gives the largest average dimensions possible for the protein.

Acknowledgements

This work has been supported in part by National Institutes of Health training grants 3T90DK070135 to D.S.W. and 5R90DK071502 to K.-P.W. and by National Institutes of Health grants GM 45302 to J. B. and GM 30580 to R.M.L. and also in part by National Science Foundation grants DBI-0403062 and DBI-0320746 to J.B.

Supplementary Data

Supplementary data associated with this article can be found, in the online version, at doi:10.1016/j.jmb.2009.06.063

References

1. Lansbury, P. T., Jr (1999). Evolution of amyloid: what normal protein folding may tell us about fibrillogenesis and disease. *Proc. Natl Acad. Sci. USA*, **96**, 3342–3344.
2. Perutz, M. F. (1999). Glutamine repeats and neurodegenerative diseases: molecular aspects. *Trends Biochem. Sci.* **24**, 58–63.
3. Dobson, C. M. (1999). Protein misfolding, evolution and disease. *Trends Biochem. Sci.* **24**, 329–332.
4. Chiti, F. & Dobson, C. M. (2006). Protein misfolding, functional amyloid, and human disease. *Annu. Rev. Biochem.* **75**, 333–366.
5. Siderowf, A. & Stern, M. (2003). Update on Parkinson disease. *Ann. Intern. Med.* **138**, 651–658.
6. Rochet, J. C. & Lansbury, P. T., Jr (2000). Amyloid fibrillogenesis: themes and variations. *Curr. Opin. Struct. Biol.* **10**, 60–68.
7. Davidson, W. S., Jonas, A., Clayton, D. F. & George, J. M. (1998). Stabilization of alpha-synuclein secondary structure upon binding to synthetic membranes. *J. Biol. Chem.* **273**, 9443–9449.
8. Jo, E., McLaurin, J., Yip, C. M., St George-Hyslop, P. & Fraser, P. E. (2000). Alpha-synuclein membrane interactions and lipid specificity. *J. Biol. Chem.* **275**, 34328–34334.
9. Abeliovich, A., Schmitz, Y., Farinas, I., Choi-Lundberg, D., Ho, W.-H., Castillo, P. E. *et al.* (2000). Mice lacking alpha-synuclein display functional deficits in the nigrostriatal dopamine system. *Neuron*, **25**, 239–252.

10. Cooper, A. A., Gitler, A. D., Cashikar, A., Haynes, C. M., Hill, K. J., Bhullar, B. *et al.* (2006). Alpha-synuclein blocks ER-Golgi traffic and Rab1 rescues neuron loss in Parkinson's models. *Science*, **313**, 324–328.
11. Jenco, J. M., Rawlingson, A., Daniels, B. & Morris, A. J. (1998). Regulation of phospholipase D2: selective inhibition of mammalian phospholipase D isoenzymes by alpha- and beta-synucleins. *Biochemistry*, **37**, 4901–4909.
12. George, J. M., Jin, H., Woods, W. S. & Clayton, D. F. (1995). Characterization of a novel protein regulated during the critical period for song learning in the zebra finch. *Neuron*, **15**, 361–372.
13. Yavich, L., Tanila, H., Vepsalainen, S. & Jakala, P. (2004). Role of alpha-synuclein in presynaptic dopamine recruitment. *J. Neurosci.* **24**, 11165–11170.
14. Wood, S. J., Wypych, J., Steavenson, S., Louis, J. C., Citron, M. & Biere, A. L. (1999). Alpha-synuclein fibrillogenesis is nucleation-dependent. Implications for the pathogenesis of Parkinson's disease. *J. Biol. Chem.* **274**, 19509–19512.
15. Eliezer, D., Kutluay, E., Bussell, R., Jr & Browne, G. (2001). Conformational properties of alpha-synuclein in its free and lipid-associated states. *J. Mol. Biol.* **307**, 1061–1073.
16. Weinreb, P. H., Zhen, W., Poon, A. W., Conway, K. A. & Lansbury, P. T., Jr (1996). NACP, a protein implicated in Alzheimer's disease and learning, is natively unfolded. *Biochemistry*, **35**, 13709–13715.
17. Uversky, V. N. (2003). A protein-chameleon: conformational plasticity of α-synuclein, a disordered protein involved in neurodegenerative disorders. *J. Biomol. Struct. Dyn.* **21**, 211–234.
18. Ulmer, T. S., Bax, A., Cole, N. B. & Nussbaum, R. L. (2005). Structure and dynamics of micelle-bound human alpha-synuclein. *J. Biol. Chem.* **280**, 9595–9603.
19. Bussell, R., Jr & Eliezer, D. (2003). A structural and functional role for 11-mer repeats in alpha-synuclein and other exchangeable lipid binding proteins. *J. Mol. Biol.* **329**, 763–778.
20. El-Agnaf, O. M., Bodles, A. M., Guthrie, D. J., Harriott, P. & Irvine, G. B. (1998). The N-terminal region of non-A beta component of Alzheimer's disease amyloid is responsible for its tendency to assume beta-sheet and aggregate to form fibrils. *Eur. J. Biochem.* **258**, 157–163.
21. Kim, T. D., Paik, S. R. & Yang, C. H. (2002). Structural and functional implications of C-terminal regions of alpha-synuclein. *Biochemistry*, **41**, 13782–13790.
22. Bertoncini, C. W., Rasia, R. M., Lamberto, G. R., Binolfi, A., Zweckstetter, M., Griesinger, C. & Fernandez, C. O. (2007). Structural characterization of the intrinsically unfolded protein beta-synuclein, a natural negative regulator of alpha-synuclein aggregation. *J. Mol. Biol.* **372**, 708–722.
23. Sung, Y. H. & Eliezer, D. (2007). Residual structure, backbone dynamics, and interactions within the synuclein family. *J. Mol. Biol.* **372**, 689–707.
24. Marsh, J. A., Singh, V. K., Jia, Z. & Forman-Kay, J. D. (2006). Sensitivity of secondary structure propensities to sequence differences between alpha- and gamma-synuclein: implications for fibrillation. *Protein Sci.* **15**, 2795–2804.
25. Bertoncini, C. W., Fernandez, C. O., Griesinger, C., Jovin, T. M. & Zweckstetter, M. (2005). Familial mutants of alpha-synuclein with increased neurotoxicity have a destabilized conformation. *J. Biol. Chem.* **280**, 30649–30652.
26. Bussell, R., Jr & Eliezer, D. (2001). Residual structure and dynamics in Parkinson's disease-associated mutants of alpha-synuclein. *J. Biol. Chem.* **276**, 45996–46003.
27. Bussell, R., Jr & Eliezer, D. (2004). Effects of Parkinson's disease-linked mutations on the structure of lipid-associated alpha-synuclein. *Biochemistry*, **43**, 4810–4818.
28. Rospigliosi, C. C., McClendon, S., Schmid, A. W., Ramlall, T. F., BarrÈ, P., Lashuel, H. A. & Eliezer, D. (2009). E46K Parkinson's-linked mutation enhances C-terminal-to-N-terminal contacts in alpha-synuclein. *J. Mol. Biol.* **388**, 1022–1032.
29. Wu, K. P., Kim, S., Fela, D. A. & Baum, J. (2008). Characterization of conformational and dynamic properties of natively unfolded human and mouse alpha-synuclein ensembles by NMR: implication for aggregation. *J. Mol. Biol.* **378**, 1104–1115.
30. Bertoncini, C. W., Jung, Y. S., Fernandez, C. O., Hoyer, W., Griesinger, C., Jovin, T. M. & Zweckstetter, M. (2005). Release of long-range tertiary interactions potentiates aggregation of natively unstructured alpha-synuclein. *Proc. Natl Acad. Sci. USA*, **102**, 1430–1435.
31. Uversky, V. N., Li, J. & Fink, A. L. (2001). Evidence for a partially folded intermediate in alpha-synuclein fibril formation. *J. Biol. Chem.* **276**, 10737–10744.
32. Dedmon, M. M., Lindorff-Larsen, K., Christodoulou, J., Vendruscolo, M. & Dobson, C. M. (2005). Mapping long-range interactions in alpha-synuclein using spin-label NMR and ensemble molecular dynamics simulations. *J. Am. Chem. Soc.* **127**, 476–477.
33. Bisaglia, M., Mammi, S. & Bubacco, L. (2009). Structural insights on physiological functions and pathological effects of alpha-synuclein. *FASEB J.* **23**, 329–340.
34. Mittag, T. & Forman-Kay, J. D. (2007). Atomic-level characterization of disordered protein ensembles. *Curr. Opin. Struct. Biol.* **17**, 3–14.
35. Eliezer, D. (2009). Biophysical characterization of intrinsically disordered proteins. *Curr. Opin. Struct. Biol.* **19**, 23–30.
36. Bracken, C., Iakoucheva, L. M., Romero, P. R. & Dunker, A. K. (2004). Combining prediction, computation and experiment for the characterization of protein disorder. *Curr. Opin. Struct. Biol.* **14**, 570–576.
37. Wright, P. E. & Dyson, H. J. (2009). Linking folding and binding. *Curr. Opin. Struct. Biol.* **19**, 31–38.
38. Vitalis, A., Wang, X. & Pappu, R. V. (2007). Quantitative characterization of intrinsic disorder in polyglutamine: insights from analysis based on polymer theories. *Biophys. J.* **93**, 1923–1937.
39. Khandogin, J. & Brooks, C. L., III (2007). Linking folding with aggregation in Alzheimer's β-amyloid peptides. *Proc. Natl Acad. Sci. USA*, **104**, 16880–16885.
40. Baumketner, A., Bernstein, S. L., Wyttenbach, T., Bitan, G., Teplow, D. B., Bowers, M. T. & Shea, J.-E. (2006). Amyloid β-protein monomer structure: a computational and experimental study. *Protein Sci.* **15**, 420–428.
41. Panchal, S. C., Bhavesh, N. S. & Hosur, R. V. (2001). Improved 3D triple resonance experiments, HNN and HN(C)N, for HN and ^{15}N sequential correlations in (^{13}C, ^{15}N) labeled proteins: application to unfolded proteins. *J. Biomol. NMR*, **20**, 135–147.
42. Mohana-Borges, R., Goto, N. K., Kroon, G. J., Dyson, H. J. & Wright, P. E. (2004). Structural characterization

of unfolded states of apomyoglobin using residual dipolar couplings. *J. Mol. Biol.* **340**, 1131–1142.
43. Kristjansdottir, S., Lindorff-Larsen, K., Fieber, W., Dobson, C. M., Vendruscolo, M. & Poulsen, F. M. (2005). Formation of native and non-native interactions in ensembles of denatured ACBP molecules from paramagnetic relaxation enhancement studies. *J. Mol. Biol.* **347**, 1053–1062.
44. Meier, S., Blackledge, M. & Grzesiek, S. (2008). Conformational distributions of unfolded polypeptides from novel NMR techniques. *J. Chem. Phys.* **128**, 052204.
45. Wilkins, D. K., Grimshaw, S. B., Receveur, V., Dobson, C. M., Jones, J. A. & Smith, L. J. (1999). Hydrodynamic radii of native and denatured proteins measured by pulse field gradient NMR techniques. *Biochemistry*, **38**, 16424–16431.
46. Neal, S., Nip, A. M., Zhang, H. & Wishart, D. S. (2003). Rapid and accurate calculation of protein ^{1}H, ^{13}C and ^{15}N chemical shifts. *J. Biomol. NMR*, **26**, 215–240.
47. Wishart, D. S. & Sykes, B. D. (1994). The ^{13}C chemical-shift index: a simple method for the identification of protein secondary structure using ^{13}C chemical-shift data. *J. Biomol. NMR*, **4**, 171–180.
48. Frishman, D. & Argos, P. (1995). Knowledge based protein secondary structure assignment. *Proteins*, **23**, 566–579.
49. Johnson, S. (1967). Hierarchical clustering schemes. *Psychometrika*, **32**, 241–254.
50. Ganguly, D. & Chen, J. Structural interpretation of paramagnetic relaxation enhancement-derived distances for disordered protein states. *J. Mol. Biol.* **390**, 467–477.
51. Uversky, V. N., Gillespie, J. R. & Fink, A. L. (2000). Why are "natively unfolded" proteins unstructured under physiologic conditions? *Proteins*, **41**, 415–427.
52. Cowan, R. & Whittaker, R. (1990). Hydrophobicity indices for amino acid residues as determined by high-performance liquid chromatography. *Pept. Res.* **3**, 75–80.
53. Hoyer, W., Cherny, D., Subramaniam, V. & Jovin, T. M. (2004). Impact of the acidic C-terminal region comprising amino acids 109–140 on alpha-synuclein aggregation in vitro. *Biochemistry*, **43**, 16233–16242.
54. Rivers, R. C., Kumita, J. R., Tartaglia, G. G., Dedmon, M. M., Pawar, A., Vendruscolo, M. *et al.* (2008). Molecular determinants of the aggregation behavior of alpha- and beta-synuclein. *Protein Sci.* **17**, 887–898.
55. Binolfi, A., Rasia, R. M., Bertoncini, C. W., Ceolin, M., Zweckstetter, M., Griesinger, C. *et al.* (2006). Interaction of alpha-synuclein with divalent metal ions reveals key differences: a link between structure, binding specificity and fibrillation enhancement. *J. Am. Chem. Soc.* **128**, 9893–9901.
56. Fernandez, C. O., Hoyer, W., Zweckstetter, M., Jares-Erijman, E. A., Subramaniam, V., Griesinger, C. & Jovin, T. M. (2004). NMR of alpha-synuclein–polyamine complexes elucidates the mechanism and kinetics of induced aggregation. *EMBO J.* **23**, 2039–2046.
57. Delaglio, F., Grzesiek, S., Vuister, G. W., Zhu, G., Pfeifer, J. & Bax, A. (1995). NMRPipe: a multidimensional spectral processing system based on UNIX pipes. *J. Biomol. NMR*, **6**, 277–293.
58. Goddard, T. D. & Kneller, D. G. Sparky 3. University of California, San Francisco, CA.
59. Ferentz, A. E. & Wagner, G. (2000). NMR spectroscopy: a multifaceted approach to macromolecular structure. *Q. Rev. Biophys.* **33**, 29–65.
60. Wishart, D. S. & Case, D. A. (2001). Use of chemical shifts in macromolecular structure determination. *Methods Enzymol.* **338**, 3–34.
61. Wishart, D. S., Bigam, C. G., Holm, A., Hodges, R. S. & Sykes, B. D. (1995).). ^{1}H, ^{13}C and ^{15}N random coil NMR chemical shifts of the common amino acids. I. Investigations of nearest-neighbor effects. *J. Biomol. NMR*, **5**, 67–81.
62. Schwarzinger, S., Kroon, G. J., Foss, T. R., Chung, J., Wright, P. E. & Dyson, H. J. (2001). Sequence-dependent correction of random coil NMR chemical shifts. *J. Am. Chem. Soc.* **123**, 2970–2978.
63. Schwarzinger, S., Kroon, G. J., Foss, T. R., Wright, P. E. & Dyson, H. J. (2000). Random coil chemical shifts in acidic 8 M urea: implementation of random coil shift data in NMRView. *J. Biomol. NMR*, **18**, 43–48.
64. Li, Y., Kim, S., Brodsky, B. & Baum, J. (2005). Identification of partially disordered peptide intermediates through residue-specific NMR diffusion measurements. *J. Am. Chem. Soc.* **127**, 10490–10491.
65. Ruckert, M. & Otting, G. (2000). Alignment of biological macromolecules in novel nonionic liquid crystalline media for NMR experiments. *J. Am. Chem. Soc.* **122**, 7793–7797.
66. Felts, A., Harano, Y., Gallichio, E. & Levy, R. (2004). Free-energy surfaces of beta hairpin and alpha-helical peptides generated by replica exchange molecular dynamics with the AGBNP implicit solvent model. *Proteins: Struct., Funct., Bioinf.* **56**, 310–321.
67. Sugita, Y. & Okamoto, Y. (1999). Replica-exchange molecular dynamics method for protein folding. *Chem. Phys. Lett.* **314**, 141–151.
68. Banks, J. L., Beard, H. S., Cao, Y., Cho, A. E., Damm, W., Farid, R. *et al.* (2005). Integrated modeling program, applied chemical theory (IMPACT). *J. Comput. Chem.* **26**, 1752–1780.
69. Gallicchio, E. & Levy, R. M. (2004). AGBNP: an analytic implicit solvent model suitable for molecular dynamics and high-resolution modeling. *J. Comput. Chem.* **25**, 479–499.
70. Kaminsky, G., Friesner, R., Tirado-Rives, J. & Jorgensen, W. (2001). Evaluation and reparametrization of the OPLS-AA force field for proteins via comparison with accurate quantum chemical calculations on peptides. *J. Phys. Chem. B*, **105**, 6474–6487.
71. Garcia de la Torre, J., Huertas, M. L. & Carrasco, B. (2000). Calculation of hydrodynamic properties of globular proteins from their atomic-level structure. *Biophys. J.* **78**, 719–730.
72. Sridharan, S., Nicholls, A. & Honig, B. (1992). A new vertex algorithm to calculate solvent accessible surface areas. *Biophys. J.* **61**, A194.

Note added in proof. The articles entitled "Charge neutralization and collapse of the C-terminal tail of alpha-synuclein at low pH" by Sebastian McClendon, Carla Rospigliosi, and David Eliezer and "Structural characterization of alpha-synuclein in an aggregation prone state" by Cho MK et al. appeared in press online in Protein Science. The work described here was carried out independently of both laboratories.